Characterization of the Interaction of Two Peptides from the N Terminus of the NHR Domain of HIV-1 gp41 with Phospholipid Membranes†

Miguel R. Moreno, Jaime Guillén, Ana J. Pérez-Berná, Diego Amorós, Ana I. Gómez, Ángela Bernabeu, and José Villalaín*

Instituto de Biología Molecular y Celular, Campus de Elche, Universidad "Miguel Hernández", E-03202 Elche-Alicante, Spain

Received May 12, 2007; Revised Manuscript Received July 5, 2007

ABSTRACT: The HIV-1 gp41 envelope glycoprotein is responsible for the membrane fusion between the virus and the target cell. According to recent models, the N-terminal coiled-coil (NHR) region of gp41 is involved in forming the interfaces between neighboring helices in the six-helix bundle, as well as in membrane binding and perturbation. In order to get new insights into the viral membrane fusion mechanism, two peptides, pFP_{15} and pFP_{23}, pertaining to the first part of the gp41 NHR domain were studied regarding their structure and their ability to induce membrane leakage, aggregation, and fusion, as well as their affinity toward specific phospholipids by a variety of spectroscopic methods. Our results demonstrate that the first part of the NHR domain interacts with negatively charged phospholipid-containing model membranes, modifies the phase behavior of membrane phospholipids, and induces leakage and aggregation of liposomes, suggesting that it could be involved directly in the merging of the viral and target cell membranes working synergistically with other membrane-active regions of the gp41 glycoprotein to boost the fusion process. On the other hand, we suggest that this region of the NHR domain could be involved in the first steps of the destabilization of the HIV-1 gp41 six-helix bundle after its interaction with negatively charged phospholipid headgroups.

The human immunodeficiency virus (HIV)[1] causes the acquired immunodeficiency syndrome by killing CD4 T-cells of the host organism (*1*−*3*). The envelope protein-induced membrane fusion of the plasma and viral membranes, mediated by gp120/gp41 envelope glycoproteins located on the outer surface of the viral membrane, enables the virus to enter into the target cells. It is thought that the gp41 envelope glycoprotein catalyzes membrane fusion through the induction of transient nonbilayer structures at the point where both bilayers merge (*1*−*4*). The gp41 sequence is highly conserved (*5*) and contains different functional regions within its ectodomain that are critical for membrane fusion, i.e., the fusion peptide, two heptad repeat regions, the Trp-rich pretransmembrane domain, and the loop domain (see Figure 1) (*6*−*10*). These regions of the gp41 glycoprotein have the capabilities of binding and partitioning into the surface of phospholipid model membranes, change their conformation, and induce the formation of nonlamellar structures, indicating that these segments could play an essential role in the viral fusion process (*6*−*15*). However, the specific mode by which these sequences get involved in membrane fusion is not well-known.

The fusion domain (FP) and N-heptad repeat (NHR) regions, along with the pretransmembrane one (PTM), are the most conserved along the gp41 ectodomain (*5*) (see Figure 1 for a scheme of the structural and functional regions of the HIV gp41 ectodomain). Specifically, the first part of the NHR region has six residues, namely, GIVQQQ, that are intimately involved in forming the three interfaces between the neighboring helices in the six-helix bundle and the interactions between them (*6*−*10*). Other conserved and interesting positions along the NHR region of the gp41 ectodomain are the so-named a and d positions (Figure 1), which are involved in trimeric coiled-coil formation, in addition to the e and g positions involved in the interactions with the CHR helices, forming the bundle of six helices (*5*, *16*). These highly conserved residues form hydrophobic cavities, which can be used as targets in the search of HIV-1

†This work was supported by Grant BFU2005-00186-BMC (Ministerio de Ciencia y Tecnología, Spain) to J.V. M.R.M. and A.B. are recipients of predoctoral fellowships from the Ministerio de Educación, Cultura y Deporte, Spain. A.J.P. and J.G. are recipients of predoctoral fellowships from the Autonomous Government of the Valencian Community, Spain.

* Corresponding author. Tel: +34 966 658 762. Fax: +34 966 658 758. E-mail: jvillalain@umh.es.

[1] Abbreviations: BPI, bovine brain L-α-phosphatidylinositol; BPS, bovine brain L-α-phosphatidylserine; CF, 5-carboxyfluorescein; CHR, C-terminal heptad repeat region; Chol, cholesterol; DEPE, 1,2-dielaidoyl-*sn*-glycero-3-phosphoethanolamine; DMPA, 1,2-dimyristoyl-*sn*-glycero-3-phosphatidic acid; DMPC, 1,2-dimyristoyl-*sn*-glycero-3-phosphatidylcholine; DMPG, 1,2-dimyristoyl-*sn*-glycero-3-phosphatidylglycerol; DMPS, 1,2-dimyristoyl-*sn*-glycero-3-phosphatidylserine; DPH, 1,6-diphenyl-1,3,5-hexatriene; EPA, egg L-α-phosphatidic acid; EPC, egg L-α-phosphatidylcholine; FPE, *N*-(fluorescein-5-thiocarbamyl)-1,2-dihexadecanoyl-*sn*-glycero-3-phosphoethanolamine; HIV, human immunodeficiency virus; LUV, large unilamellar vesicles; MLV, multilamellar vesicles; NBD-PE, *N*-(7-nitrobenz-2-oxa-1,3-diazol-4-yl)-1,2-dihexadecanoyl-*sn*-glycero-3-phosphoethanolamine; NHR, N-terminal heptad repeat region; N-RhB-PE, lissamine rhodamine B 1,2-dihexadecanoyl-*sn*-glycero-3-phosphoethanolamine; PA-DPH, 1,6-diphenyl-1,3,5-hexatrienepropionic acid; pFP_{15}, postfusion peptide 15-mer; pFP_{23}, postfusion peptide 23-mer; POPE, 1-palmitoyl-2-oleoyl-*sn*-glycero-3-phosphoethanolamine; PTM, pretransmembrane; SM, egg sphingomyelin; SUV, small unilamellar vesicles; ThT, thioflavin T; TMA-DPH, 1-(4-trimethylammoniumphenyl)-6-phenyl-1,3,5-hexatriene; TPE, egg trans-esterified L-α-phosphatidylethanolamine.

10.1021/bi700911g CCC: $37.00
Published on Web 08/21/2007

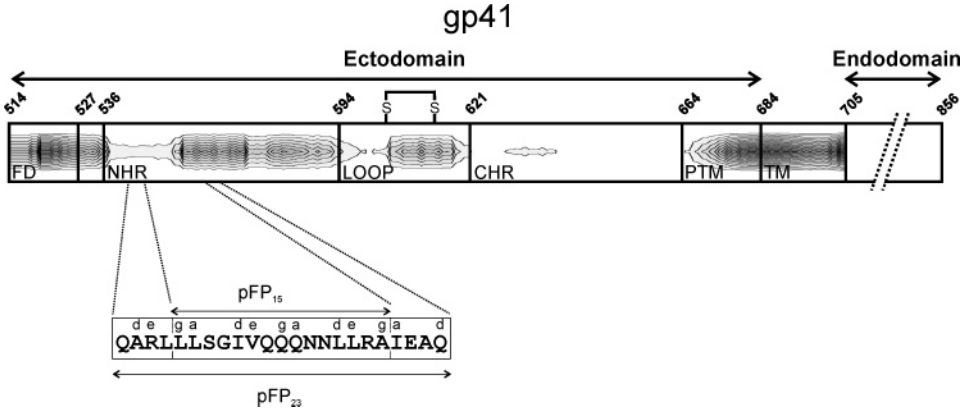

FIGURE 1: Scheme of the HIV_{MN} gp41 ectodomain showing the structural and functional regions as well as their relative lengths. The fusion domain (FP), the loop, the NHR and CHR heptad repeats, the pretransmembrane stretch (PTM), and the transmembrane (TM) domain have been drawn approximately to scale. The residue numbers correspond to their positions in gp160 of the HIV_{MN} strain, whereas the sequence and location of the gp41 fragments studied in this work are indicated. The summation of the normalized experimental values corresponding to membrane rupture, phospholipid mixing, and fusion are overlapped (the darker, the greater the membranotropic effect) along the gp41 ectodomain sequence (see ref *11*). Heptad-repeat positions are labeled a through g.

inhibitors. For instance, T-20 is a peptide pertaining to the CHR/PTM regions of gp41, which binds competitively, at least, to the first part of the NHR (*17*, *18*), blocking efficiently the six-helix bundle formation, prerequisite for the fusion and viral entry (*19*, *20*). Significantly, mutated HIV-1 strains having mutations in the first part of the NHR region are resistant to T-20 (*21*, *22*). On the other hand, previous studies have shown that the NHR region is involved directly in membrane binding and perturbation, boosts the fusogenic capability of the FP region, and modulates oligomerization and increase in phospholipid mixing (*14*, *23*). Significantly, the NHR region undergoes a shift to an extended structure from the α-helix upon interaction with negatively charged membranes, leading to a pronounced fusion activity (*14*, *24*).

Viral membrane fusion is an important research topic since it serves as a model for cellular fusion events and it is a very good target for therapeutic intervention (*4*); however, although much information has been gathered in recent years, we do not know yet the different processes and mechanism of membrane fusion. Elucidating the nature of the interactions between phospholipid membranes and membrane proteins is important for the understanding of the structure and function of the implicated biomolecules as well as the mechanism which underlies membrane fusion. In the present work we describe a comparative biophysical study of the membrane interaction of two peptides corresponding to the early part of the NHR region of the gp41 ectodomain immediately adjacent to the fusion domain incorporating within them the sequence GIVQQQ (Figure 1), one of them comprising a length of 15 amino acids (pFP_{15}) and the other one elongated four amino acids at each side of the previous one (pFP_{23}). It is the purpose of the present work to study these fragments in the presence of different membrane model systems composed of different phospholipid mixtures, to evaluate its incorporation and location in the membrane model systems, and to study its effect on the integrity and phase behavior of the membrane. Our results demonstrate that this region of the NHR domain binds and interacts with negatively charged membranes, which suggest that it could be involved directly in merging of the viral and cellular membranes and might work synergistically with other membrane-active regions of the gp41 glycoprotein to boost the fusion process as has been recently shown by Korazim et al. (*24*).

MATERIALS AND METHODS

Materials and Reagents. The HIV envelope protein gp41 fragments encompassing residues 545−559 (^{545}LLSGIVQQQNNLLRA^{559}, pFP_{15}) and 541−563 (^{541}QARLLLSGIVQQQNNLLRAIEAQ^{563}, pFP_{23}) of strain HIV_{MN} were synthesized with C-terminal amide and N-terminal acetylation on an automatic multiple synthesizer (Genemed Synthesis). The peptides were purified by reverse-phase HPLC (Vydac C-8 column, 250 × 4.6 mm, flow rate 1 mL/min, solvent A, 0.1% trifluoroacetic acid, solvent B, 99.9% acetonitrile and 0.1% trifluoroacetic acid) to better than 95% purity, and its composition and molecular mass were confirmed by amino acid analysis and mass spectroscopy. Egg L-α-phosphatidylcholine (EPC), egg sphingomyelin (SM), egg trans-sterified L-α-phosphatidylethanolamine (TPE), egg L-α-phosphatidic acid (EPA), bovine brain L-α-phosphatidylserine (BPS), bovine brain L-α-phosphatidylinositol (BPI), 1,2-dimyristoyl-*sn*-glycero-3-phosphatidylcholine (DMPC), 1,2-dimyristoyl-*sn*-glycero-3-phosphatidylglycerol (DMPG), 1-palmitoyl-2-oleoyl-*sn*-glycero-3-phosphoethanolamine (POPE), 1,2-dielaidoyl-*sn*-glycero-3-phosphoethanolamine (DEPE), 1,2-dimyristoyl-*sn*-glycero-3-phosphatidylserine (DMPS), 1,2-dimyristoyl-*sn*-glycero-3-phosphatidic acid (DMPA), and cholesterol (Chol) were obtained from Avanti Polar Lipids (Alabaster, AL). *N*-(Fluorescein-5-thiocarbamyl)-1,2-dihexadecanoyl-*sn*-glycero-3-phosphoethanolamine (FPE), lissamine rhodamine B 1,2-dihexadecanoyl-*sn*-glycero-3-phosphoethanolamine (N-RhB-PE), *N*-(7-nitrobenz-2-oxa-1,3-diazol-4-yl)-1,2-dihexadecanoyl-*sn*-glycero-3-phosphoethanolamine (NBD-PE), 1,6-diphenyl-1,3,5-hexatriene (DPH), 1-(4-trimethylammoniumphenyl)-6-phenyl-1,3,5-hexatriene (TMA-DPH), and 1,6-diphenyl-1,3,5-hexatrienepropionic acid (PA-DPH) were obtained from Molecular Probes Inc. (Eugene, OR). 5-Carboxyfluorescein (CF) (>95% by HPLC) was from Sigma-Aldrich (Madrid, Spain). Sodium dithionite was from Fluka (Darmstadt, Germany). All other chemicals were commercial samples of the highest purity available (Sigma-Aldrich, Madrid,

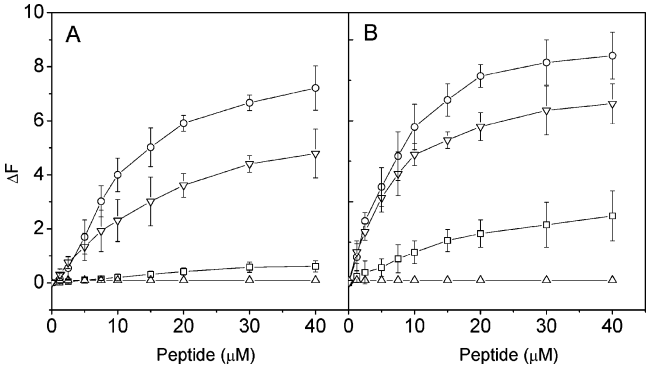

FIGURE 2: Effect of peptide concentration on the fluorescence signal amplitude of FPE by pFP_{15} (A) and pFP_{23} (B). The lipid concentration was 200 μM. The phospholipid compositions were EPC:Chol at a molar ratio of 5:1 (△), EPC:BPS:Chol at a molar ratio of 5:4:1 (□), EPC:SM:Chol at a molar ratio of 5:1:1 (▽), and EPC:TPE:SM:BPI:BPS:EPA:Chol at a molar ratio of 46.4:21.2:8.8:4.4:9.3:0.81:9.1 (○). Vertical bars indicate standard deviations of the mean of triplicate samples.

Spain). Water was deionized, twice distilled, and passed through Milli-Q equipment (Millipore Ibérica, Madrid, Spain) to a resistivity better than 18 MΩ·cm.

Sample Preparation. Aliquots containing the appropriate amount of lipid in chloroform/methanol (2:1 v/v) were placed in a test tube, the solvents were removed by evaporation under a stream of O_2-free nitrogen, and, finally, traces of solvents were eliminated under vacuum in the dark for more than 3 h. The lipid films were resuspended in an appropriate buffer and incubated either at 25 °C or at 10 °C above the phase transition temperature (T_m) with intermittent vortexing for 30 min to hydrate the samples and obtain multilamellar vesicles (MLV). The samples were frozen and thawed five times to ensure complete homogenization and maximization of peptide/lipid contacts with occasional vortexing. Large unilamellar vesicles (LUV) with a mean diameter of 0.1 and 0.2 μm were prepared from multilamellar vesicles by the extrusion method (*25*) using polycarbonate filters with a pore size of 0.1 and 0.2 μm (Nuclepore Corp., Cambridge, CA). Small unilamellar vesicles (SUV) were prepared from MLVs using a Branson 250 sonifier (40W) equipped with a microtip until the suspension became completely transparent. Every 30 s, the samples were cooled for 90 s in ice to prevent overheating of the solution. The titanium particles released from the tip were removed by centrifugation at 15000 rpm at room temperature for 15 min. The phospholipid and peptide concentrations were measured by methods described previously (*26, 27*). The peptides pFP_{15} and pFP_{23} were dissolved in buffer containing 50% and 25% DMSO, respectively. The maximum DMSO concentration in the final solution was always lower than 1%. The complex membrane simulating the lymphocyte plasma membrane was composed of EPC:TPE:SM:BPI:BPS:EPA:Chol at a molar ratio of 46.4:21.2:8.8:4.4:9.3:0.81:9.1 (*28, 29*).

Fluorescence Measurements Using FPE-Labeled Membranes. LUVs with a mean diameter of 0.1 μm were prepared in buffer containing 10 mM Tris-HCl, pH 7.4. The vesicles were labeled exclusively in the outer bilayer leaflet with FPE as described previously (*30*). Briefly, LUVs were incubated with 0.1 mol % FPE dissolved in ethanol (never more than 0.1% of the total aqueous volume) at 37 °C for 1 h in the dark. Any remaining unincorporated FPE was removed by gel filtration on a Sephadex G-25 column equilibrated with the appropriate buffer. FPE vesicles were stored at 4 °C until use in an oxygen-free atmosphere. Fluorescence time courses of FPE-labeled vesicles were measured after the desired amount of peptide was added into 400 μL of lipid suspensions (200 μM lipid) using a Varian Cary Eclipse fluorescence spectrometer. Excitation and emission wavelengths were set at 490 and 520 nm, respectively, using excitation and emission slits set at 5 nm. Temperature was controlled with a thermostatic bath at 25 °C. The contribution of light scattering to the fluorescence signals was measured in experiments without the dye and was subtracted from the fluorescence traces. Data were fitted either to a hyperbolic or to a sigmoidal binding model (*31*) using the equations:

$$F = \frac{F_{max}[pFP]}{K_d + [pFP]} \quad \text{or} \quad F = \frac{F_{max}[pFP]^n}{K_d^n + [pFP]^n} \quad (1)$$

where F is the fluorescence variation, F_{max} the maximum fluorescence variation, [pFP] the peptide concentration, K_d the dissociation constant of the membrane binding process, and n the Hill coefficient.

Liposome Aggregation. LUVs with a mean diameter of 0.1 μm were prepared in buffer containing 10 mM Tris-HCl, pH 7.4. Changes in aggregation state of the vesicles were monitored by absorbance measurement at 436 nm (*32*). Aliquots of peptide stock solutions were added to 400 μL suspensions of LUV (lipid concentration, 200 μM) in Tris-HCl, pH 7.4, in a 10 mm × 10 mm cuvette. The absorbance was measured using a Beckman DU-640 spectrophotometer before and after the addition of the peptide. The contribution of light scattering of peptide solutions without lipid vesicles was subtracted from their corresponding values of absorbance after peptide addition in the presence of lipid vesicles.

Membrane Leakage Measurement. LUVs with a mean diameter of 0.1 μm were prepared in buffer containing 10 mM Tris-HCl, 20 mM NaCl, 40 mM CF, and 0.05 mM EDTA, pH 7.4. Nonencapsulated CF was separated from the vesicle suspension through a Sephadex G-75 filtration column (Pharmacia, Uppsala, Sweden) eluted with buffer containing 10 mM Tris-HCl, 100 mM NaCl, and 0.05 mM EDTA, pH 7.4. Membrane rupture (leakage) of intraliposomal CF was assayed by treating the probe-loaded liposomes (final lipid concentration 75 μM) with the appropriate amounts of peptide in a 5 mm × 5 mm fluorescence cuvette stabilized at 25 °C under constant stirring, with a final volume of 400 μL (75 μM lipid concentration). Changes in fluorescence intensity were recorded on a Varian Cary Eclipse fluorescence spectrometer with excitation and emission wavelengths set at 492 and 517 nm, respectively. Excitation and emission slits were set at 5 nm. One hundred percent release was achieved by adding Triton X-100 to a final concentration of 0.5% (w/w) to the fluorescence cuvette. Fluorescence measurements were made initially with probe-loaded liposomes and afterward by adding peptide solution and finally adding Triton X-100 to obtain 100% leakage. Leakage was quantified on a percentage basis according to the equation:

$$\%\, L = \frac{(F_f - F_0) \times 100}{F_{100} - F_0} \quad (2)$$

where F_f is the equilibrium value of fluorescence after peptide addition, F_0 the initial fluorescence of the vesicle suspension, and F_{100} the fluorescence value after addition of Triton X-100.

Phospholipid-Mixing Measurement. Peptide-induced vesicle lipid mixing was measured by resonance energy transfer (*33*). This assay is based on the decrease in resonance energy transfer between two probes (NBD-PE and RhB-PE) when the lipids of the probe-containing vesicles are allowed to mix with lipids from vesicles lacking the probes. The concentration of each of the fluorescent probes within the liposome membrane was 0.6 mol %. LUVs with a mean diameter of 0.2 μm were prepared as described above. Labeled and unlabeled vesicles in a proportion of 1:4 were placed in a 5 mm $\times$ 5 mm fluorescence cuvette at a final lipid concentration of 100 μM in a final volume of 400 μL, stabilized at 25 °C under constant stirring. The fluorescence was measured using a Varian Cary Eclipse fluorescence spectrometer using 467 and 530 nm for excitation and emission, respectively. Excitation and emission slits were set at 10 nm. Since labeled and unlabeled vesicles were mixed in a proportion of 1 to 4, respectively, 100% phospholipid mixing was estimated with a liposome preparation in which the membrane concentration of each probe was 0.12%. Phospholipid mixing was quantified on a percentage basis according to the equation:

$$\%\ \mathrm{PM} = \frac{(F_f - F_0) \times 100}{F_{100} - F_0} \quad (3)$$

where F_f is the value of fluorescence obtained 15 min after peptide addition to a liposome mixture containing liposomes having 0.6% of each probe plus liposomes without any fluorescent probe, F_0 the initial fluorescence of the vesicles, and F_{100} the fluorescence value of the liposomes containing 0.12% of each probe.

Inner-Monolayer Phospholipid-Mixing (Fusion) Measurement. Peptide-induced phospholipid mixing of the inner monolayer was measured by a modification of the phospholipid-mixing measurement stated above (*34*). LUVs were treated with sodium dithionite to completely reduce the NBD-labeled phospholipid located at the outer monolayer of the membrane. The final concentration of sodium dithionite was 100 mM (from a stock solution of 1 M dithionite in 1 M Tris-HCl, pH 10.0), and the mixture was incubated for approximately 1 h on ice in the dark. Sodium dithionite was then removed by size exclusion chromatography through a Sephadex G-75 filtration column (Pharmacia, Uppsala, Sweden) eluted with buffer containing 10 mM Tris-HCl, 100 mM NaCl, and 1 mM EDTA, pH 7.4. The proportion of labeled and unlabeled vesicles, lipid concentration, and other experimental and measurement conditions were the same as indicated above for the phospholipid mixing assay.

Steady-State Fluorescence Anisotropy. DPH and its derivatives represent popular membrane fluorescent probes for monitoring the organization and dynamics of membranes; while DPH is known to partition mainly into the hydrophobic core of the membrane, PA-DPH and TMA-DPH probes are oriented at the membrane bilayer with their charge localized at the lipid−water interface, TMA-DPH nearer the membrane surface than PA-DPH (*35*). MLVs were formed in 100 mM NaCl, 0.05 mM EDTA, and 25 mM HEPES, pH 7.4. Aliquots of PA-DPH, TMA-DPH, or DPH in *N*,*N*′-dimethylformamide (2×10^{-4} M) were directly added into the lipid dispersion to obtain a probe:lipid molar ratio of 1:500. Samples were incubated for 15, 45, or 60 min when TMA-DPH, PA-DPH, or DPH was used, respectively, 10 °C above the gel to liquid-crystalline phase transition temperature T_m of the phospholipid mixture. Afterward, the peptides were added to obtain a peptide:lipid molar ratio of 1:15 and incubated 10 °C above the T_m of each lipid for 1 h, with occasional vortexing. All fluorescence studies were carried using 5 mm $\times$ 5 mm quartz cuvettes in a final volume of 400 μL (315 μM lipid concentration). All of the data were corrected for background intensities and progressive dilution. The steady-state fluorescence anisotropy, $\langle r \rangle$, was measured with an automated polarization accessory using a Varian Cary Eclipse fluorescence spectrometer, coupled to a Peltier device (Varian) for automatic temperature change. The vertically and horizontally polarized emission intensities, elicited by vertically polarized excitation, were corrected for background scattering by subtracting the corresponding polarized intensities of a phospholipid preparation lacking probes. The *G*-factor, accounting for differential polarization sensitivity, was determined by measuring the polarized components of the fluorescence of the probe with horizontally polarized excitation ($G = I_{HV}/I_{HH}$). Samples were excited at 360 nm (slit width, 5 nm), and fluorescence emission was recorded at 430 nm (slit width, 5 nm). The values were calculated from the equation (*36*). The steady-state anisotropy was defined by equation:

$$\langle r \rangle = \frac{(I_{VV} - GI_{VH})}{(I_{VV} + 2GI_{VH})} \quad (4)$$

where I_{VV} and I_{VH} are the measured fluorescence intensities (after appropriate background subtraction) with the excitation polarizer vertically oriented and the emission polarizer vertically and horizontally oriented, respectively.

Thioflavin T Assays for Peptide Aggregation. Peptide aggregation was assayed by using thioflavin T (ThT). Thioflavin T associates rapidly with aggregated peptides, giving rise to a new excitation maximum at 450 nm and a enhanced emission at 482 nm (*37*). Buffer contained 100 mM NaCl, 10 mM Tris-HCl, 25 μM ThT, pH 7.4, either SDS (final concentration of 8 mM) or LUVs (final phospholipid concentration of 0.5 mM), and a peptide concentration of 5 μM. Fluorescence was measured before and after the desired amount of peptide was added into the cuvette using a Varian Cary Eclipse fluorescence spectrometer. Temperature was controlled with a thermostatic bath at 25 °C under constant stirring. Samples were excited at 450 nm (slit width, 5 nm), and the fluorescence emission was recorded at 482 nm (slit width, 5 nm). Aggregation was quantified on a percentage basis according to the equation:

$$\%\, A = \frac{(F_f - F_0) \times 100}{F_{max} - F_0} \quad (5)$$

where F_f is the value of fluorescence after peptide addition, F_0 the initial fluorescence in the absence of peptide, and F_{max}

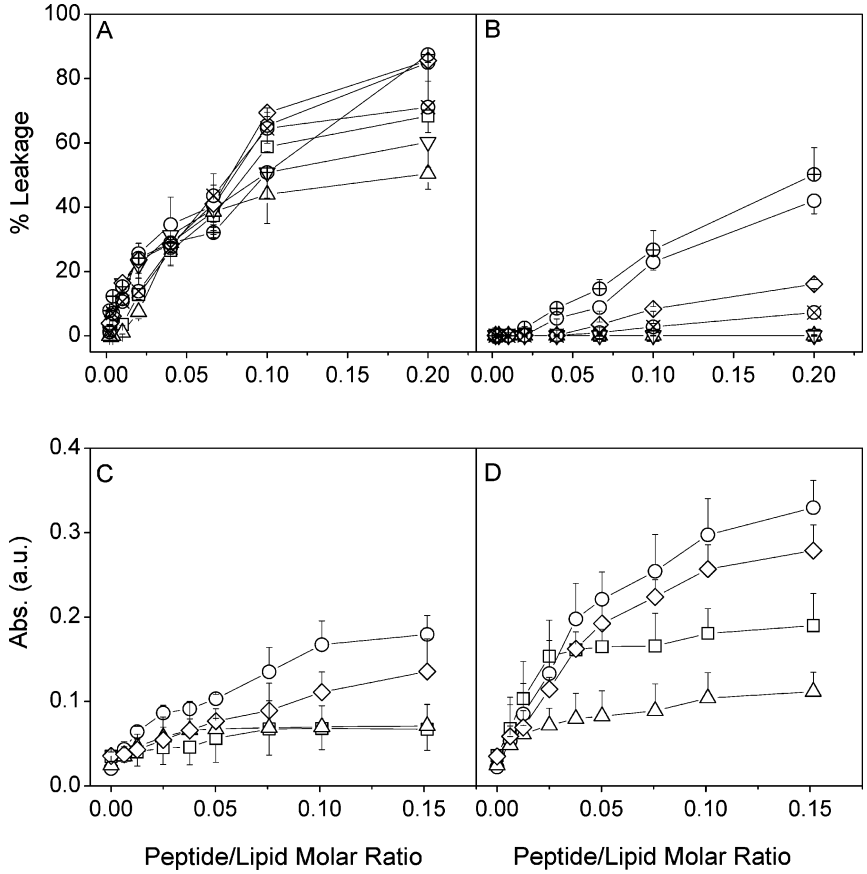

FIGURE 3: Effect of pFP_{15} (A, C) and pFP_{23} (B, D) on the rupture (leakage) (A, B) and aggregation (C, D) of LUVs containing different lipid compositions at different lipid-to-peptide molar ratios. LUVs were composed of (□) EPC:Chol at a molar ratio of 5:1, (○) EPC:BPS:Chol at a molar ratio of 5:4:1, (△) EPC:SM:Chol at a molar ratio of 5:1:1, (◇) PC:PE:SM:PI:PS:PA:Chol at a molar ratio of 46.4:21.2:8.8:4.4:9.3:0.81:9.1, (▽) EPC:TPE:Chol at a molar ratio of 5:3:1, (⊕) EPC:BPI:Chol at a molar ratio of 5:4:1, and (⊗) EPC:EPG:Chol at a molar ratio of 5:4:1. Vertical bars indicate standard deviations of the mean of triplicate samples.

Table 1: Dissociation Constant (K_D), Saturation Point, and Hill Coefficient Derived from the Best Fitting of the Data from Figure 2 to Eqs 1 or 2

peptide	model membranes	binding profile	R^2	saturation point	K_D (μM)	Hill coeff
pFP_{15}	EPC:Chol (5:1)	sigmoidal	0.998	1.27	38.2	1.20
	EPC:BPS:Chol (5:4:1)	sigmoidal	0.998	7.52	9.67	1.82
	EPC:SM:Chol (5:1:1) complex membrane[a]	sigmoidal	0.999	6.94	18.4	1.09
pFP_{23}	EPC:Chol (5:1)	hyperbolic	0.997	3.79	22.1	
	EPC:BPS:Chol (5:4:1)	sigmoidal	0.998	9.85	7.39	1.16
	EPC:SM:Chol (5:1:1) complex membrane[a]	hyperbolic	0.999	8.03	7.64	

[a] Composed of EPC:TPE:SM:BPI:BPS:EPA:Chol at a molar ratio of 46.4:21.2:8.8:4.4:9.3:0.81:9.1.

the fluorescence maximum obtained immediately after peptide addition.

Circular Dichroism Spectroscopy. SUVs were prepared in 100 μM phosphate, pH 7.4. Different concentrations of trifluoroethanol (TFE) and sodium dodecyl sulfate (SDS), both below and above the critical micellar concentration, as well as SUVs of EPC or BPS to attain different peptide-to-lipid ratios were added to the corresponding samples. Each cuvette contained 40 μg of peptide. Spectra were measured at 25 °C on a Jasco J-810 CD spectropolarimeter fitted with a thermostatically controlled cell holder and interfaced with a Neslab RTE-111 water bath, using a 2 mm path length cell. Wavelength spectra were acquired every 0.2 nm at a scan speed of 50 nm·min^{-1} with a response time of 2 s and averaged over five scans at 25 °C from 250 to 190 nm, with a bandwidth of 2 nm. Secondary structure predictions were estimated using the software CDNN 2.1 (*38*).

RESULTS

We have shown recently the existence of different membranotropic regions of the gp41 envelope glycoprotein ecto- and endodomains by using a library of 15-mer peptides encompassing the full sequence of the gp41 envelope glycoprotein (*11*). One of these membranotropic regions was located at the beginning of the NHR domain just contiguous to the fusion domain (Figure 1). Since this region could be important in the membrane fusion process (*14*, *23*, *24*), we present here the results of the study of the interaction with model membranes of two peptides derived from this region, one of them having 15 amino acid residues (pFP_{15}) and the

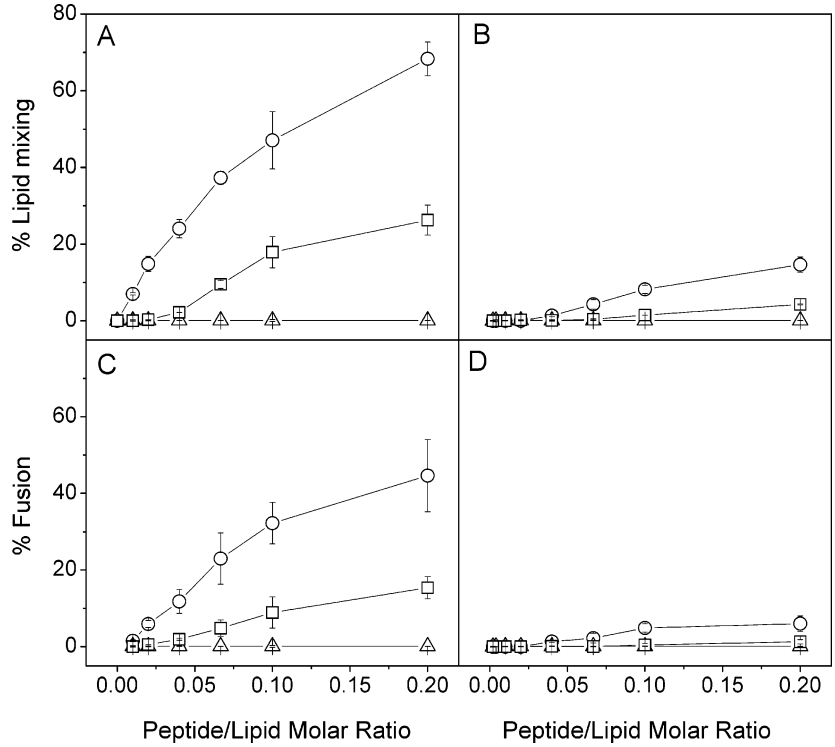

FIGURE 4: Effect of (A, C) pFP_{15} and (B, D) pFP_{23} on phospholipid mixing (A, B) and membrane fusion (C, D) of LUVs having different lipid compositions at different lipid-to-peptide molar ratios. LUVs were composed of (□) EPC:BPS:Chol at a molar ratio of 5:4:1, (○) EPC:SM:Chol at a molar ratio of 5:1:1, and (△) EPC:TPE:SM:BPI:BPS:EPA:Chol at a molar ratio of 46.4:21.2:8.8:4.4:9.3:0.81:9.1. Vertical bars indicate standard deviations of the mean of triplicate samples.

other one having four amino acids more at both ends of the former one (pFP_{23}) (Figure 1).

Since both peptides lack a Trp residue, we have used the electrostatic surface potential probe FPE (*39*) to monitor their ability to bind to model membranes composed of different lipid compositions at different lipid/peptide ratios (Figure 2). Both peptides had a higher affinity for model membranes containing negatively charged phospholipids, i.e., EPC/BPS/Chol and the complex membrane simulating lymphocyte plasma membranes (*28*, *29*). Interestingly, very little or no effect was observed for liposomes composed of EPC/Chol and EPC/SM/Chol. The smallest dissociation constant and the biggest saturation point for both pFP_{15} and pFP_{23} were found in the presence of model membranes containing EPC/BPS/Chol. Except for pFP_{15} in the presence of EPC/BPS/Chol model membranes, all other cases could be adjusted to a binding profile having either a sigmoidal (Hill coefficient of approximately 1) or a hyperbolic dependence (Table 1), which might suggest that the interaction of the peptide with the membrane was monomeric. For pFP_{15} in the presence of EPC/BPS/Chol-containing membranes a sigmoidal dependence with a Hill coefficient of approximately 1.82 could be observed (Table 1), suggesting that the interaction of the peptide with this negatively charged membrane could be through a dimeric form of the peptide.

The extent of carboxyfluorescein leakage induced by pFP_{15} and pFP_{23} peptides on model membranes having different lipid compositions as a function of peptide:lipid ratio is given in Figure 3A,B. It can be observed that pFP_{15} induced a greater membrane destabilization than pFP_{23} in all of the different samples tested. Interestingly, pFP_{15} induced nearly a 90% leakage at a lipid-to-peptide ratio of 5 on liposomes containing EPC/Chol plus either BPI or BPS as well as on the model membrane resembling the lymphocyte plasma membrane (Figure 3A). Smaller but significant leakage values were found for the other compositions tested. In contrast to pFP_{15}, it is interesting to note that pFP_{23} hardly exerted any effect on liposomes containing EPC/Chol plus either SM or TPE, i.e., compositions containing no negatively charged phospholipids. However, both peptides, although to different extents, induced a greater extent of leakage on membranes composed of negatively charged phospholipids. It is interesting to highlight that both peptides have the same net positive charge of +1 at pH 7.4. However, the distribution of charges along the sequence is different, since pFP_{15} has only one charge at the end of the sequence whereas pFP_{23} is charged at both ends of the sequence. It would be plausible then that pFP_{15} could destabilize membranes by inserting into the membrane more easily than pFP_{23} through the noncharged part of its sequence. It should be noted that although pFP_{15}-induced leakage was higher than pFP_{23} for all lipid compositions, pFP_{23} membrane binding was slightly larger than that observed for pFP_{15} (Figure 2).

Since membrane apposition is a necessary requisite before true membrane fusion can occur (*40*), the ability of pFP_{15} and pFP_{23} to induce vesicle aggregation was tested in order to investigate whether this property correlated with the peptide-membrane binding and leakage assays. The changes in the absorbance at 432 nm of different liposome compositions as a function of the peptide-to-lipid molar ratio are shown in Figure 3C,D. The data revealed that there was a good correlation between aggregation and binding assays, since the highest membrane binding was found, and the highest aggregation effect was observed. In this case, pFP_{23} was capable of binding to membranes to a higher extent than pFP_{15}, so that higher aggregation was observed for pFP_{23}

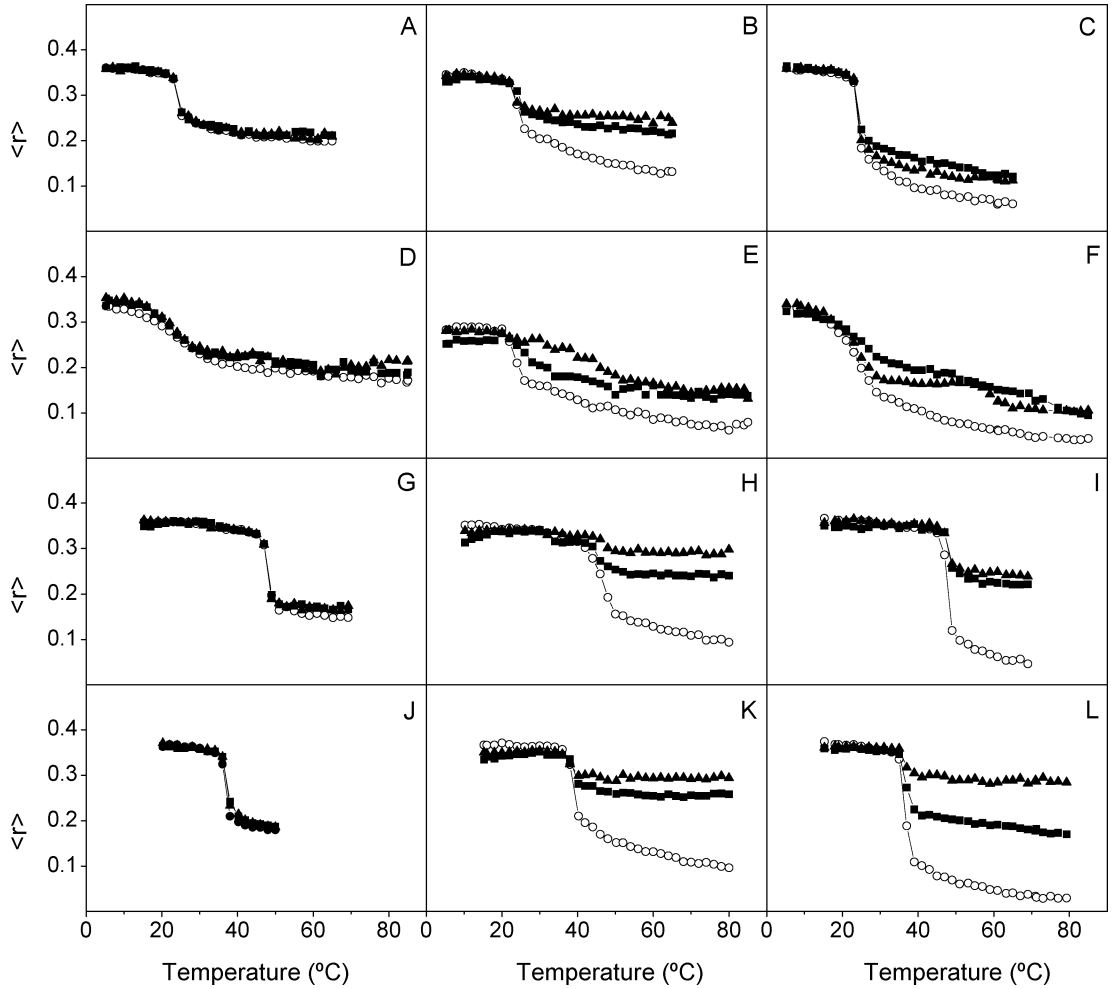

FIGURE 5: Steady-state anisotropy, $\langle r \rangle$, of TMA-DPH (A, D, G, J), PA-DPH (B, E, H, K), and DPH (C, F, I, L) as a function of temperature for MLVs composed of DMPC (A, B, C), POPE (D, E, F), DMPA (G, H, I), and DMPS (J, K, L) in the absence (○) and in the presence of pFP_{15} (■) and pFP_{23} (▲) at a phospholipid:peptide molar ratio of 15:1.

than for pFP_{15}. It is also interesting to note that the presence of negatively charged phospholipids favored the aggregation process, the highest aggregation value being observed for EPC/BPS/Chol-containing liposomes.

Membrane fusion requires at least two distinct processes, binding or apposition of membranes and the subsequent merger of these membranes (*40*). The induction of intervesicular lipid mixing and inner-monolayer lipid mixing by the peptides, as a measure of their fusogenic activity, was tested with several types of vesicles utilizing the probe dilution assay (*33*, *34*). The dependence of the extent of both processes on pFP_{23} and pFP_{15} concentration was examined as observed in Figure 4. It became evident that only the pFP_{15} peptide could induce significant lipid mixing and inner-monolayer lipid mixing in the presence of liposomes composed of negatively charged phospholipids but not with zwitterionic ones. The maximum values for both lipid mixing and membrane fusion were obtained for the EPC/BPS/Chol lipid composition with pFP_{15}, since percentage values of 68% and 45% were observed for mixing and fusion, respectively (Figure 4A,C), in contrast to the values observed for pFP_{23} (15% and 6%, respectively) (Figure 4B,D). It would be possible that the membrane mixing and fusion effect observed for pFP_{23} in contrast to that observed for pFP_{15} could be due to the same reasoning explained above for the differences observed for leakage. We have observed until now the highest effect on liposomes containing negatively charged phospholipids; however, Chol was present in all samples. To confirm that the high membranotropic activity was due to the negative charge on the membrane surface but not to cholesterol (*41*, *42*), we carried out intervesicular lipid mixing and inner-monolayer lipid mixing with liposomes composed of EPC:BPS at a molar ratio of 5:4 (data not shown), obtaining similar results to liposomes composed of EPC/BPS/Chol.

The effect of the gp41-derived peptides on the structural and thermotropic properties of phospholipid membranes was further investigated by measuring the steady-state fluorescence anisotropy of the fluorescent probes DPH, PA-DPH, and TMA-DPH incorporated into DMPC, POPE, DMPA, and DMPS membranes as a function of temperature (Figure 5). As observed in Figure 5, the presence of either pFP_{23} or pFP_{15} did not induce any significant effect neither on the anisotropy both below and above the T_m of the phospholipids nor on the cooperativity of the transition when the TMA-DPH probe was used. However, significant changes were observed for the anisotropy of both PA-DPH and DPH above, but not below, the phospholipid main transition. The presence of both peptides, pFP_{23} and pFP_{15}, induced an increase of the anisotropies when compared with the pure phospholipids, suggesting that the peptides were able to decrease the mobility of the phospholipid acyl chains above but not below

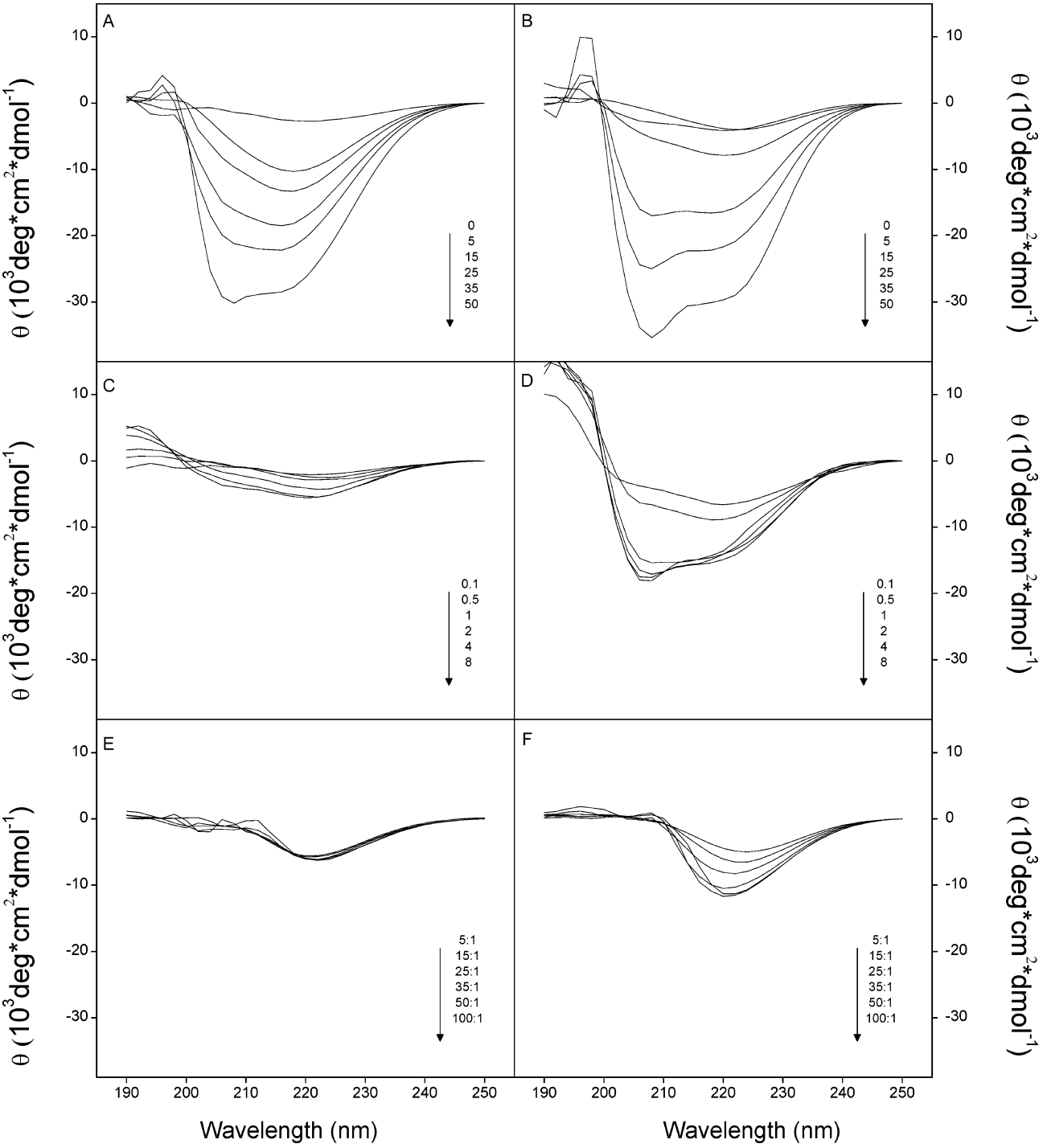

FIGURE 6: CD spectra of pFP_{15} (A, C, E) and pFP_{23} (B, D, F) in TFE (A, B), SDS (C, D), and SUVs of BPS (E, F). The percentages of TFE, the SDS concentration in mM, and the lipid-to-peptide ratio are indicated. The temperature was 25 °C.

the T_m. It is also interesting to note that the observed effect on the anisotropies was greater for negatively charged phospholipids than for zwitterionic ones, in agreement with the data commented above. When the effects induced by the two peptides were compared, it was observed that peptide pFP_{23} induced a bigger effect than peptide FP_{15} on membranes containing negatively charged phospholipids (see Figure 5). The increase in anisotropy observed above T_m for the fluorescent probes PA-DPH and DPH when compared with TMA-DPH would indicate that both peptides would insert in the membrane when the phospholipid phase is in the liquid-crystalline phase but not in the gel phase, where the peptides would be at the membrane surface. However, it should not be ruled out that the positively charged TMA-DPH probe could be moved away from the positive charge of the peptides, whereas this would not be the case for the negatively charged PA-DPH probe, explaining in part the lack of any observed effect for TMA-DPH in the presence of both peptides. Nevertheless, these data demonstrate that both peptides affect the fluidity behavior of these phospholipids. Taking into account these results together with the ones commented above, it could be suggested that both peptides, pFP_{23} and pFP_{15}, although interacting with the membrane, should be located at the lipid−water interface.

The secondary structures of both peptides pFP_{23} and pFP_{15} were analyzed by circular dichroism (CD) (Figure 6). In

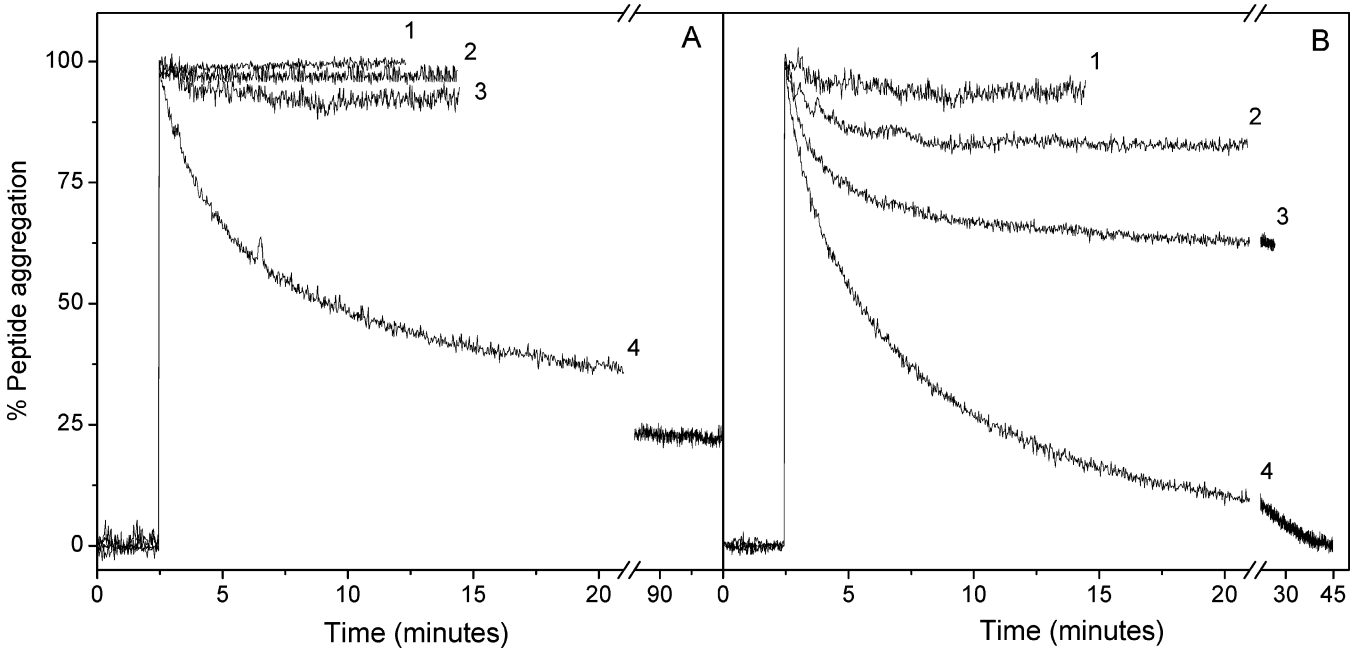

FIGURE 7: Percentage of aggregation of pFP_{15} (A) and pFP_{23} (B) in the absence (1) and in the presence of EPC (2), BPS (3), and SDS (4). See text for details.

aqueous buffer, both peptides were mainly aggregated, as assessed by both CD (Figure 6A,B) and infrared spectroscopy (data not shown). By infrared the amide I′ band presented an intense absorption maximum at 1621 cm^{-1} and a less intense maximum at 1687 cm^{-1}, characteristic of extended β-strands with strong intermolecular interactions (*43*). In the presence of 5−15% of TFE, both peptides presented a relatively high β-sheet content and random structure (Figure 6A,B). However, the α-helical content of both peptides increased as the concentration of TFE increased (Figure 6A,B). The data indicated that pFP_{23} had a slightly higher helical content than pFP_{15} for the same TFE concentration (80% and 67%, respectively, at 50% TFE). The presence of increasing concentrations of SDS hardly exerted any effect on the aggregation state of pFP_{15}, but it increased the α-helical content of pFP_{23} so that about 40% was found at the maximum SDS concentration studied (Figure 6C,D). When different concentrations of SUVs of EPC were used, no effect was observed for both pFP_{23} and pFP_{15} when compared with the peptides in solution (data not shown). The same happened when SUVs of BPS were added to pFP_{15} (Figure 6E). However, an increase in random coil, according to the secondary structure prediction estimated by the software CDNN 2.1 (*38*), was observed for pFP_{23}. This spectrum change could suggest that pFP_{23} aggregation was decreased in the presence of this negatively charged phospholipid (Figure 6F).

Finally, the peptide aggregation state for both peptides was assayed using ThT (*37*). As observed in Figure 7A, pFP_{15} remained mainly aggregated in the presence of both EPC and BPS but not in the presence of SDS (about 25% of aggregation). However, the aggregation of pFP_{23} was diminished in the presence of either EPC or BPS (about 83% and 62% aggregation, respectively) when compared to SDS (no aggregation) (see Figure 7B). Interestingly, the extent of aggregation was smaller when both peptides were in the presence of BPS than in the presence of EPC (clearer for pFP_{23} than for pFP_{15}), suggesting again that the interaction of both pFP_{15} and pFP_{23} with negatively charged phospholipids was different than with zwitterionic ones.

DISCUSSION

The membrane fusion protein of HIV is the envelope transmembrane gp41 glycoprotein, and it is thought that several gp41 proteins are capable of juxtaposing, destabilizing, and merging the viral and cellular membranes so that a fusion pore is formed (*1*, *2*, *40*, *44*−*46*). A lot of research, not only on gp41 but also on other viral membrane fusion proteins, points out that these proteins have several regions which are involved in the fusion process. Destabilization of the lipid bilayer and membrane fusion appears then to be the result of the binding and interaction of different segments of fusion proteins with biological membranes. However, little is known about how the complex series of protein/protein and protein/phospholipid interactions drive membrane apposition and how they overcome the energy barriers for membrane fusion (*1*, *2*, *11*, *24*, *47*−*49*). Even though many studies have been carried out on the interaction of synthetic peptides mimicking the N-terminal fusion peptide and the Trp-rich membrane proximal regions of gp41 with model membranes, fewer studies have examined the interaction of other segments of the gp41 protein with phospholipid vesicles. Importantly, new targets for inhibition of gp41-mediated membrane fusion may be discovered by obtaining structural information on both the native and fusion-intermediate conformations of gp41 and its segments. Although it is unquestionable that the fusion peptide of gp41 plays an essential role at the beginning of the membrane fusion process (*1*−*4*), other works have also shown that the fusion activity of FP is increased by the postfusion peptide (*14*, *23*, *47*, *50*). On the basis of our recent work (*11*), we have selected the N-terminal region of the NHR domain of gp41 to carry out a biophysical study, aiming to elucidate the capacity of this region, adjacent to the fusion domain, to interact and disrupt membranes with an approach based on different but complementary strategies: membrane rupture,

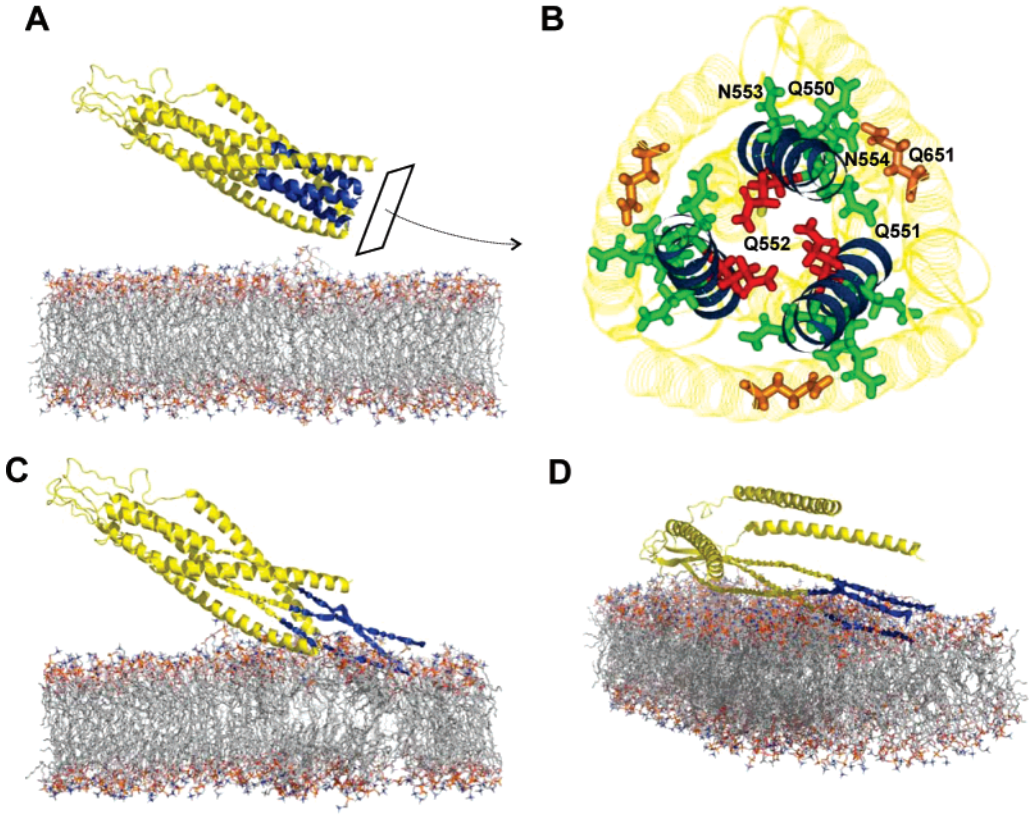

FIGURE 8: Schematic model of the destabilization of the six-helix bundle of gp41. (A) Depiction of the gp41 six-helix bundle showing the NHR, CHR, and loop domains and a membrane bilayer. The first part of the NHR domain is indicated (blue). (B) Front view of the gp41 ectodomain without the FD and PTM domains, indicating in detail the spatial arrangement of the amino acids pertaining to the sequence ^{550}QQQNN^{554}. While Q552 is located at the interior of the coiled coil (red), the other residues are situated in the exterior part (green). Q651 belongs to the CHR domain of gp41 and forms a hydrogen bond with Q550 (orange). (C) The early part of the NHR domain would interact with the negatively charged phospholipid headgroups located at the membrane surface, and the α-helical structure would begin to unfold and destabilize the coiled coil. (D) Both the six-helix bundle and coiled-coil conformations would be completely unfolded, while the NHR domain would show a nonhelical structure or an extended structure according to Korazim et al. (*24*), which would remain in contact with the membrane surface. Presumably, this gp41 structure, through the destabilization of the membrane bilayer, should be the fusogenic one. The structure of the gp41 coiled coil is based on the Protein Data Bank accession code 1IF3, whereas the membrane is represented as a simulated model of a POPC bilayer in the fluid phase (*64*). The diagrams were modeled using the PyMOL Molecular Graphics System.

mixing and fusion, liposome and peptide aggregation, and peptide structure.

The pFP_{15} and pFP_{23} peptides studied in this work bind with high affinity to phospholipid model membranes containing negatively charged phospholipids. We and others have previously found similar binding affinities for other peptides pertaining to the loop and NHR regions of the gp41 protein (*8*, *9*, *12*, *24*, *51*). The main binding force was apparently from an electrostatic origin, presumably owing to the net charge of +1 for each peptide. We have also previously shown that the predominant charge of the NHR and loop regions of the gp41 ectodomain is positive, whereas the CHR and pretransmembrane regions are negative (*11*). Comparing both peptide activities, we have observed that pFP_{15} induces a higher effect in membrane leakage, lipid mixing, and fusion except for liposome aggregation. This effect could be due to the high hydrophobic character of pFP_{15} with respect to pFP_{23}. On the other hand, pFP_{15}, in comparison with pFP_{23}, has the N-terminal free of charged amino acids, so that the pFP_{15} N-terminal part can insert itself into the lipid bilayer deeper into the membrane interface. On the other hand, pFP_{23} has a greater liposome aggregation effect than pFP_{15}, probably because pFP_{23} should be located at the membrane surface.

We have shown that both pFP_{15} and pFP_{23} are capable of affecting the steady-state fluorescence anisotropy of fluorescent probes located in the palisade structure of the membrane. Both peptides increase the membrane order above the main transition temperature of different phospholipid types, predominantly to negatively charged phospholipids. In agreement with these results, they do not modify the transition enthalpy as observed by DSC though they slightly increase the main transition temperature of negative phospholipids. Interestingly, pFP_{23} induces the presence of two components in the thermogram corresponding to DMPS, indicating the presence of at least two phospholipid populations. It is also worth noting that both peptides shift, although slightly, the fluid-lamellar phase to the hexagonal type H_{II} phase transition, suggesting that they could aid in the promotion of nonlamellar lipid structures. As observed by CD and IR, both pFP_{15} and pFP_{23} presented a large proportion of random and aggregated structures. However, TFE, a stabilizing agent of predominant secondary structures in polypeptides (*52*), is capable of inducing a significant increase of α-helical structure, suggesting that these peptides could adopt, given the right conditions, this type of structure. In the presence of EPC both peptides did not present any significant difference, but the presence of BPS induced, more

significantly for pFP_{23} than for pFP_{15}, the appearance of another type of structure, indicating that this negatively charged phospholipid could reduce peptide aggregation. This is corroborated by the ThT assays, which indicate that both peptides disaggregate more efficiently in the presence of BPS than in the presence of EPC.

Taking together all of these results, and in accordance with other studies (*9*, *24*, *53*, *54*), the NHR domain of gp41 would interact predominantly with negatively charged phospholipids. It is also known that several FP fragments pertaining to different gp41 trimers can provoke the formation of local nipples in the cell plasmatic membrane (*55*), leading to the formation of local bends which could induce zones of nonlamellar phases on the outer leaflet. The outer leaflet of the target cell is composed predominantly of zwitterionic phospholipids whereas the inner leaflet is highly negatively charged. It would be possible that the imbalance produced by a different phospholipid assembly in the inner leaflet with respect to the outer leaflet would produce phospholipid flip-flop from the inner leaflet to the outer leaflet to satisfy the packing restrictions (*56*). The present data would suggest that disassembly of the core could possibly happen only after exposure to negatively charged membranes, either by flip-flop or when in contact with the inner leaflet. In this way, the NHR region could interact, according to Korazim et al. (*24*), with the negatively charged outer leaflet favoring the fusion process mediated by gp41, leading to the fusogenic pore formation. This should be possible because the energy which is liberated when the NHR trimer interacts with the membrane is capable of initiating the conformational changes which drive to the NHR monomeric form (*57*); the NHR monomeric form in turn would interact with the membrane surface through its hydrophobic part. This is feasible given that both NHR and CHR domains could be free to interact with the membrane (*58*), since presumably bundle formation occurs after the fusion pore has formed (*59*). Electrostatic interactions between the NHR domain, which has a positive net charge, and negatively charged phospholipid headgroups could be the main ones in the first moment. However, it is also interesting to note the large quantity of conserved Q and N residues in the NHR domain (*5*), the majority of them located in the first part of it, which could contribute to the stabilization of the NHR/negatively charged phospholipid complex by the formation of a number of intermolecular hydrogen bonds, similarly to other proteins (*60*). According to all of these data, it could be considered that the beginning of the NHR region could initiate the destabilization of the gp41 coiled coil in the presence of negatively charged phospholipids (Figure 8). This hypothesis would be based on that (1) the mutation of residue Q^{651} from the CHR domain, which forms hydrogen bonds with Q^{550} and N^{554}, decreases gp41-mediated membrane fusion (*61*), (2) the Q^{552} residue buried inside a coiled-coil conformation can decrease the interaction force between helices, even facilitating the reversibility of the coiled-coil formation (*62*), (3) sequences from the NHR domain which interact with negatively charged phospholipids possess the ^{550}QQQNN^{554} sequence (*24*, *63*), (4) the coiled coil is destabilized in the presence of negatively charged phospholipid-containing membranes (*24*, *63*), and (5) the data described in this work shows that peptides derived from this NHR domain interact and destabilize membranes containing preferentially negatively charged phospholipids. Since it has been previously suggested that gp41 hairpin folding drives the fusion reaction by apposing the viral and cellular membranes together as well as by initiating pore formation (*2*, *14*, *15*, *59*), it could be considered that this region of the gp41 ectodomain during and/or after the fusion process could interact with the CHR region immediately adjacent to the pretransmembrane one and, therefore, might be essential for the assistance and enhancement of the viral and cell fusion process.

ACKNOWLEDGMENT

We thank Prof. J. M. Sanz for fruitful discussions on circular dichroism.

REFERENCES

1. Eckert, D. M., and Kim, P. S. (2001) Mechanisms of viral membrane fusion and its inhibition, *Annu. Rev. Biochem. 70*, 777−810.
2. Gallo, S. A., Finnegan, C. M., Viard, M., Raviv, Y., Dimitrov, A., Rawat, S. S., Puri, A., Durell, S., and Blumenthal, R. (2003) The HIV Env-mediated fusion reaction, *Biochim. Biophys. Acta 1614*, 36−50.
3. Markovic, I., and Clouse, K. A. (2004) Recent advances in understanding the molecular mechanisms of HIV-1 entry and fusion: revisiting current targets and considering new options for therapeutic intervention, *Curr. HIV Res. 2*, 223−234.
4. Earp, L. J., Delos, S. E., Park, H. E., and White, J. M. (2005) The many mechanisms of viral membrane fusion proteins, *Curr. Top. Microbiol. Immunol. 285*, 25−66.
5. Dong, X. N., Xiao, Y., Dierich, M. P., and Chen, Y. H. (2001) N- and C-domains of HIV-1 gp41: mutation, structure and functions, *Immunol. Lett. 75*, 215−220.
6. Bosch, M. L., Earl, P. L., Fargnoli, K., Picciafuoco, S., Giombini, F., Wong-Staal, F., and Franchini, G. (1989) Identification of the fusion peptide of primate immunodeficiency viruses, *Science 244*, 694−697.
7. Gallaher, W. R., Ball, J. M., Garry, R. F., Griffin, M. C., and Montelaro, R. C. (1989) A general model for the transmembrane proteins of HIV and other retroviruses, *AIDS Res. Hum. Retroviruses 5*, 431−440.
8. Pascual, R., Moreno, M. R., and Villalain, J. (2005) A peptide pertaining to the loop segment of human immunodeficiency virus gp41 binds and interacts with model biomembranes: implications for the fusion mechanism, *J. Virol. 79*, 5142−5152.
9. Pascual, R., Contreras, M., Fedorov, A., Prieto, M., and Villalain, J. (2005) Interaction of a peptide derived from the N-heptad repeat region of gp41 Env ectodomain with model membranes. Modulation of phospholipid phase behavior, *Biochemistry 44*, 14275−14288.
10. Suarez, T., Nir, S., Goni, F. M., Saez-Cirion, A., and Nieva, J. L. (2000) The pre-transmembrane region of the human immunodeficiency virus type-1 glycoprotein: a novel fusogenic sequence, *FEBS Lett. 477*, 145−149.
11. Moreno, M. R., Giudici, M., and Villalain, J. (2006) The membranotropic regions of the endo and ecto domains of HIV gp41 envelope glycoprotein, *Biochim. Biophys. Acta 1758*, 111−123.
12. Contreras, L. M., Aranda, F. J., Gavilanes, F., Gonzalez-Ros, J. M., and Villalain, J. (2001) Structure and interaction with membrane model systems of a peptide derived from the major epitope region of HIV protein gp41: implications on viral fusion mechanism, *Biochemistry 40*, 3196−3207.
13. Peisajovich, S. G., Epand, R. F., Pritsker, M., Shai, Y., and Epand, R. M. (2000) The polar region consecutive to the HIV fusion peptide participates in membrane fusion, *Biochemistry 39*, 1826−1833.
14. Sackett, K., and Shai, Y. (2002) The HIV-1 gp41 N-terminal heptad repeat plays an essential role in membrane fusion, *Biochemistry 41*, 4678−4685.
15. Dimitrov, A. S., Rawat, S. S., Jiang, S., and Blumenthal, R. (2003) Role of the fusion peptide and membrane-proximal domain in HIV-1 envelope glycoprotein-mediated membrane fusion, *Biochemistry 42*, 14150−14158.

16. Jiang, S., Lin, K., Zhang, L., and Debnath, A. K. (1999) A screening assay for antiviral compounds targeted to the HIV-1 gp41 core structure using a conformation-specific monoclonal antibody, *J. Virol. Methods 80*, 85−96.
17. Liu, S., Lu, H., Niu, J., Xu, Y., Wu, S., and Jiang, S. (2005) Different from the HIV fusion inhibitor C34, the anti-HIV drug Fuzeon (T-20) inhibits HIV-1 entry by targeting multiple sites in gp41 and gp120, *J. Biol. Chem. 280*, 11259−11273.
18. Chang, D. K., and Hsu, C. S. (2007) Biophysical evidence of two docking sites of the carboxyl heptad repeat region within the amino heptad repeat region of gp41 of human immunodeficiency virus type 1, *Antiviral Res. 74*, 51−58.
19. Chen, C. H., Matthews, T. J., McDanal, C. B., Bolognesi, D. P., and Greenberg, M. L. (1995) A molecular clasp in the human immunodeficiency virus (HIV) type 1 TM protein determines the anti-HIV activity of gp41 derivatives: implication for viral fusion, *J. Virol. 69*, 3771−3777.
20. Kilgore, N. R., Salzwedel, K., Reddick, M., Allaway, G. P., and Wild, C. T. (2003) Direct evidence that C-peptide inhibitors of human immunodeficiency virus type 1 entry bind to the gp41 N-helical domain in receptor-activated viral envelope, *J. Virol. 77*, 7669−7672.
21. Lohrengel, S., Hermann, F., Hagmann, I., Oberwinkler, H., Scrivano, L., Hoffmann, C., von Laer, D., and Dittmar, M. T. (2005) Determinants of human immunodeficiency virus type 1 resistance to membrane-anchored gp41-derived peptides, *J. Virol. 79*, 10237−10246.
22. Mink, M., Mosier, S. M., Janumpalli, S., Davison, D., Jin, L., Melby, T., Sista, P., Erickson, J., Lambert, D., Stanfield-Oakley, S. A., Salgo, M., Cammack, N., Matthews, T., and Greenberg, M. L. (2005) Impact of human immunodeficiency virus type 1 gp41 amino acid substitutions selected during enfuvirtide treatment on gp41 binding and antiviral potency of enfuvirtide in vitro, *J. Virol. 79*, 12447−12454.
23. Wexler-Cohen, Y., Sackett, K., and Shai, Y. (2005) The role of the N-terminal heptad repeat of HIV-1 in the actual lipid mixing step as revealed by its substitution with distant coiled coils, *Biochemistry 44*, 5853−5861.
24. Korazim, O., Sackett, K., and Shai, Y. (2006) Functional and structural characterization of HIV-1 gp41 ectodomain regions in phospholipid membranes suggests that the fusion-active conformation is extended, *J. Mol. Biol. 364*, 1103−1117.
25. Mayer, L. D., Hope, M. J., and Cullis, P. R. (1986) Vesicles of variable sizes produced by a rapid extrusion procedure, *Biochim. Biophys. Acta 858*, 161−168.
26. Böttcher, C. S. F., Van Gent, C. M., and Fries, C. (1961) A rapid and sensitive sub-micro phosphorus determination, *Anal. Chim. Acta 1061*, 203−204.
27. Edelhoch, H. (1967) Spectroscopic determination of tryptophan and tyrosine in proteins, *Biochemistry 6*, 1948−1954.
28. Brugger, B., Glass, B., Haberkant, P., Leibrecht, I., Wieland, F. T., and Krausslich, H. G. (2006) The HIV lipidome: a raft with an unusual composition, *Proc. Natl. Acad. Sci. U.S.A. 103*, 2641−2646.
29. Aloia, R. C., Tian, H., and Jensen, F. C. (1993) Lipid composition and fluidity of the human immunodeficiency virus envelope and host cell plasma membranes, *Proc. Natl. Acad. Sci. U.S.A. 90*, 5181−5185.
30. Wall, J., Ayoub, F., and O'Shea, P. (1995) Interactions of macromolecules with the mammalian cell surface, *J. Cell Sci. 108* (Part 7), 2673−26782.
31. Golding, C., Senior, S., Wilson, M. T., and O'Shea, P. (1996) Time resolution of binding and membrane insertion of a mitochondrial signal peptide: correlation with structural changes and evidence for cooperativity, *Biochemistry 35*, 10931−10937.
32. Persson, D., Thoren, P. E., and Norden, B. (2001) Penetratin-induced aggregation and subsequent dissociation of negatively charged phospholipid vesicles, *FEBS Lett. 505*, 307−312.
33. Struck, D. K., Hoekstra, D., and Pagano, R. E. (1981) Use of resonance energy transfer to monitor membrane fusion, *Biochemistry 20*, 4093−4099.
34. Meers, P., Ali, S., Erukulla, R., and Janoff, A. S. (2000) Novel inner monolayer fusion assays reveal differential monolayer mixing associated with cation-dependent membrane fusion, *Biochim. Biophys. Acta 1467*, 227−243.
35. Lentz, B. R. (1993) Use of fluorescent probes to monitor molecular order and motions within liposome bilayers, *Chem. Phys. Lipids 64*, 99−116.
36. Lakowicz, J. (1999) *Principles of Fluorescence Spectroscopy*, Kluwer-Plenum Press, New York.
37. LeVine, H., III (1993) Thioflavine T interaction with synthetic Alzheimer's disease beta-amyloid peptides: detection of amyloid aggregation in solution, *Protein Sci. 2*, 404−410.
38. Bohm, G., Muhr, R., and Jaenicke, R. (1992) Quantitative analysis of protein far UV circular dichroism spectra by neural networks, *Protein Eng. 5*, 191−195.
39. Wall, J., Golding, C. A., Van Veen, M., and O'Shea, P. (1995) The use of fluoresceinphosphatidylethanolamine (FPE) as a real-time probe for peptide-membrane interactions, *Mol. Membr. Biol. 12*, 183−192.
40. Blumenthal, R., Clague, M. J., Durell, S. R., and Epand, R. M. (2003) Membrane fusion, *Chem. Rev. 103*, 53−69.
41. Chen, Z., and Rand, R. P. (1997) The influence of cholesterol on phospholipid membrane curvature and bending elasticity, *Biophys. J. 73*, 267−276.
42. Churchward, M. A., Rogasevskaia, T., Hofgen, J., Bau, J., and Coorssen, J. R. (2005) Cholesterol facilitates the native mechanism of Ca^{2+}-triggered membrane fusion, *J. Cell Sci. 118*, 4833−4848.
43. Arrondo, J. L., and Goni, F. M. (1999) Structure and dynamics of membrane proteins as studied by infrared spectroscopy, *Prog. Biophys. Mol. Biol. 72*, 367−405.
44. Colman, P. M., and Lawrence, M. C. (2003) The structural biology of type I viral membrane fusion, *Nat. Rev. Mol. Cell Biol. 4*, 309−319.
45. LeDuc, D. L., and Shin, Y. K. (2000) Insights into a structure-based mechanism of viral membrane fusion, *Biosci. Rep. 20*, 557−570.
46. Weissenhorn, W., Dessen, A., Calder, L. J., Harrison, S. C., Skehel, J. J., and Wiley, D. C. (1999) Structural basis for membrane fusion by enveloped viruses, *Mol. Membr. Biol. 16*, 3−9.
47. Sackett, K., Wexler-Cohen, Y., and Shai, Y. (2006) Characterization of the HIV N-terminal fusion peptide-containing region in context of key gp41 fusion conformations, *J. Biol. Chem. 281*, 21755−21762.
48. Perez-Berna, A. J., Moreno, M. R., Guillen, J., Bernabeu, A., and Villalain, J. (2006) The membrane-active regions of the hepatitis C virus E1 and E2 envelope glycoproteins, *Biochemistry 45*, 3755−3768.
49. Guillen, J., Perez-Berna, A. J., Moreno, M. R., and Villalain, J. (2005) Identification of the membrane-active regions of the severe acute respiratory syndrome coronavirus spike membrane glycoprotein using a 16/18-mer peptide scan: implications for the viral fusion mechanism, *J. Virol. 79*, 1743−1752.
50. Sackett, K., and Shai, Y. (2003) How structure correlates to function for membrane associated HIV-1 gp41 constructs corresponding to the N-terminal half of the ectodomain, *J. Mol. Biol. 333*, 47−58.
51. Rabenstein, M., and Shin, Y. K. (1995) A peptide from the heptad repeat of human immunodeficiency virus gp41 shows both membrane binding and coiled-coil formation, *Biochemistry 34*, 13390−13397.
52. Buck, M. (1998) Trifluoroethanol and colleagues: cosolvents come of age. Recent studies with peptides and proteins, *Q. Rev. Biophys. 31*, 297−355.
53. Larsen, C. E., Nir, S., Alford, D. R., Jennings, M., Lee, K. D., and Duzgunes, N. (1993) Human immunodeficiency virus type 1 (HIV-1) fusion with model membranes: kinetic analysis and the role of lipid composition, pH and divalent cations, *Biochim. Biophys. Acta 1147*, 223−236.
54. Larsen, C. E., Alford, D. R., Young, L. J., McGraw, T. P., and Duzgunes, N. (1990) Fusion of simian immunodeficiency virus with liposomes and erythrocyte ghost membranes: effects of lipid composition, pH and calcium, *J. Gen. Virol. 71* (Part 9), 1947−1955.
55. Dimitrov, A. S., Xiao, X., Dimitrov, D. S., and Blumenthal, R. (2001) Early intermediates in HIV-1 envelope glycoprotein-mediated fusion triggered by CD4 and co-receptor complexes, *J. Biol. Chem. 276*, 30335−30341.
56. Janmey, P. A., and Kinnunen, P. K. (2006) Biophysical properties of lipids and dynamic membranes, *Trends Cell Bioll 16*, 538−456.
57. Kliger, Y., and Levanon, E. Y. (2003) Cloaked similarity between HIV-1 and SARS-CoV suggests an anti-SARS strategy, *BMC Microbiol 3*, 20.

58. Shnaper, S., Sackett, K., Gallo, S. A., Blumenthal, R., and Shai, Y. (2004) The C- and the N-terminal regions of glycoprotein 41 ectodomain fuse membranes enriched and not enriched with cholesterol, respectively, *J. Biol. Chem. 279*, 18526−18534.
59. Markosyan, R. M., Cohen, F. S., and Melikyan, G. B. (2003) HIV-1 envelope proteins complete their folding into six-helix bundles immediately after fusion pore formation, *Mol. Biol. Cell 14*, 926−938.
60. Bollinger, J. G., Diraviyam, K., Ghomashchi, F., Murray, D., and Gelb, M. H. (2004) Interfacial binding of bee venom secreted phospholipase A2 to membranes occurs predominantly by a nonelectrostatic mechanism, *Biochemistry 43*, 13293−13304.
61. Suntoke, T. R., and Chan, D. C. (2005) The fusion activity of HIV-1 gp41 depends on interhelical interactions, *J. Biol. Chem. 280*, 19852−19857.
62. Eckert, D. M., Malashkevich, V. N., and Kim, P. S. (1998) Crystal structure of GCN4-pIQI, a trimeric coiled coil with buried polar residues, *J. Mol. Biol. 284*, 859−865.
63. Kliger, Y., Peisajovich, S. G., Blumenthal, R., and Shai, Y. (2000) Membrane-induced conformational change during the activation of HIV-1 gp41, *J. Mol. Biol. 301*, 905−914.
64. Heller, H., Schaefer, M., and Schulte, K. (1993) Molecular dynamics simulation of a bilayer of 200 lipids in the gel and in the liquid crystal phases, *J. Phys. Chem. 97*, 8343−8360.

BI700911G